Journal of ETA Maritime Science

Research on Hydrodynamic Properties of a New Porous Floating Breakwater

Ouoc Hung Vu¹, Minh Tuan Vu¹, Anh-Dan Nguyen², Tri Mai³

¹Hanoi University of Civil Engineering, Faculty of Hydraulic Engineering, Hanoi, Vietnam ²University of Transport and Communications, Faculty of Civil Engineering, Hanoi, Vietnam ³Hanoi University of Civil Engineering, Faculty of Coastal and Offshore Engineering, Hanoi, Vietnam

Abstract

The growing demand for resilient and environmentally adaptive coastal protection solutions has spurred research into innovative floating breakwater (FB) designs. This study introduces and evaluates the hydrodynamic performance of a newly developed H-type porous FB (TFB-3), which incorporates perforated vertical plates to enhance energy dissipation. Using a series of physical model experiments, the TFB-3's performance is compared with two established FB designs: the conventional rectangular TFB-1 and the modified semicircular TFB-2. Experimental results demonstate that TFB-3 significantly outperforms both reference models in attenuating wave energy. Specifically, TFB-3 exhibits lower wave transmission and reflection coefficients, greater energy dissipation, and reduced wave disturbance in front of the structure. These improvements are particularly relevant for deployment in soft-soil coastal regions, where traditional breakwaters are often impractical. The findings highlight the potential of TFB-3 as a robust and scalable solution for coastal protection under a range of wave conditions. This work contributes valuable experimental data and practical insights to inform the design and application of advanced porous FBs.

Keywords: Floating breakwater, experimental study, coefficient of wave transmission, coefficient of wave reflection, coefficient of wave energy dissipation, coefficient of wave disturbance

1. Introduction

During this century, the global economic boom has driven a substantial demand for large-tonnage vessels and deepwater ports capable of accommodating these vessels for efficient cargo loading and unloading [1]. Breakwaters present an effective solution for such ports, as they not only create calm water areas for vessel mooring but also reduce wave reflection on the seaward side. However, the use of conventional rubble mound breakwaters in deep-water areas may be economically inefficient and poses significant risks to the seabed. Tutuarima and d'Angremond [2] compared the construction cost of various breakwater types under similar site conditions in hypothetical scenarios. Their findings indicate that the rubble mound breakwaters, caissons, and composite breakwaters are suitable for water depths of up to 8 m, 8 m - 20 m and 20 m - 30 m, respectively. Despite their structural effectiveness, these impermeable breakwaters often disrupt longshore sediment transport and limit water exchange. This can lead to sediment accretion on the updrift side of the structure and erosion on the downdrift side due to sediment deficit. Therefore, an ideal breakwater should not only effectively dissipate wave energy and function well in deep water, but also allow for sediment and water exchange, thereby minimizing environmental impacts. Furthermore, global climate change and sea level rise-primarily driven by thermal expansion and the melting of glaciers and mountain ice-are projected to accelerate during the 21st century, with current estimates exceeding 2.0 mm/year [3]. These changes are contributing to higher sea levels, increased wave heights, and more frequent severe weather events (e.g., storms, cyclones, and tropical depressions), which intensify coastal erosion. Since sea level rise is an irreversible trend, there is a growing demand for larger, higher and heavier breakwaters and shore protection structures to safeguard harbor basins



Address for Correspondence: Minh Tuan Vu, Hanoi University of Civil Engineering, Faculty of Hydraulic Engineering, Hanoi, Vietnam

E-mail: tuanvm@huce.edu.vn

ORCID iD: orcid.org/0000-0002-6099-0603

Received: 16.11.2024 Last Revision Received: 19.07.2025 Accepted: 15.10.2025

Epub: 20.11.2025

To cite this article: Q. H. Vu, M. T. Vu, A.-D. Nguyen, and T. Mai, "Research on hydrodynamic properties of a new porous floating breakwater." *Journal of ETA Maritime Science*, [Epub Ahead of Print]



and ship mooring areas. Nevertheless, many major portssuch as Lach Huyen Port (Vietnam) [4], Laem Chabang Port (Thailand) [5], Patimban Port (Indonesia) [6], and East Port Said Port (Egypt) [7]-are located in coastal plains underlain by soft alluvial soil. Constructing protective structures in these geotechnically challenging areas presents significant technical and economic difficulties.

Some scholars have recommended the use of submerged or floating breakwaters (FBs) as appropriate measures for reducing incident wave energy to desirable levels while enabling the free exchange of sediment and water, particularly in areas with weak ground conditions [8-10]. The most notable advantage of submerged breakwaterscontributing to their widespread adoption-is their minimal impact on beach aesthetics and recreational functions [11]. Additionally, they exert limited influence on the surrounding marine environment while still providing wave protection on their lee side. These structures also promote water circulation, help maintain longshore sediment transport, mitigate downdrift erosion, reduce stagnant water zones, and improve water quality. However, submerged breakwaters have some limitations. Their wave dissipation efficiency tends to decrease under severe weather conditions or significant sea level fluctuations. Furthermore, due to their gravity-based design-requiring massive structural weight-most submerged breakwaters are unsuitable for soft-soil foundations. They are also less effective in deep water or regions with large tidal variations. Climate change-induced sea level rise further compromises their wave attenuation performance. In contrast, FBs may offer a more suitable alternative in such contexts. They are capable of dissipating wave energy, adapting to sea level changes, and permitting minimal disruption to water exchange and sediment transport. Most importantly, they have negligible impact on the seabed and surrounding ecosystems. Numerous studies [12-17] have confirmed that FBs perform effectively under normal sea conditions. However, their efficiency and structural stability under extreme marine conditions remain areas requiring further research and validation.

Enhancing the stability and efficiency of FBs has become a central focus for researchers worldwide. Most FBs reduce transmitted wave height primarily through wave reflection. However, excessive wave reflection not only increases structural loads, anchor line tensions, and connection requirements between modules, but also poses a risk to nearby maritime operations. To mitigate reflected waves, many studies have explored energy dissipation mechanisms that rely on friction and porosity. Cho [15] investigated the interaction between rectangular FB with porous side plates and waves using a two-dimensional linear potential theory model. Compared with impermeable side plates

[18], researchers found that deeper protruded plates and optimized porosity were found to lower wave transmission coefficients. Nonetheless, considerable overtopping occurred under high-wave conditions. Christensen et al. [19] applied both physical and numerical models to evaluate damping mechanisms in modified box-shaped FBs. Their results indicated that attaching wing plates to regular pontoons significantly reduced both displacement and wave transmission/reflection. Similarly, Zheng et al. [20] reported that porous FB decreased the coefficient of transmission from 0.5% to 4% compared to a conventional model under long waves with small amplitudes. However, both studies highlighted limitations such as excessive overtopping and the need for larger structures to ensure buoyancy. To address these challenges, Tuan et al. [21] experimentally compared a perforated semi-circular FB (TFB-2) with a conventional rectangular FB (TFB-1) of equal material and weight under random wave conditions. TFB-2 demonstrated greater wave attenuation (1.3% to 7.6% improvement), but also resulted in higher reflected waves (1% to 13% increase). Further efforts to improve the performance of FB were made by Shen et al. [22], who proposed a twin-pontoon FB with multi-porous vertical plates. While this design significantly reduced the wave transmission coefficient, its reflection coefficient remained higher than that of traditional single-pontoon FB. In a more recent study, Hu et al. [23] numerically examined an FB with integrated porous baffles. The results showed improved wave energy dissipation and reduced motion amplitude; however, wave reflection was still higher than with conventional box-shaped FBs. These findings underscore that while notable progress has been made in enhancing FB designs, developing structures that can simultaneously reduce incident wave energy, minimize wave overtopping, and limit wave reflection remains an ongoing research challenge.

To address the aforementioned limitations of existing FB structures and build upon the research on the pi-type FB with porous side plates, by Cho [15], this study proposes and develops a novel porous H-type FB structure, referred to as TFB-3. Perforated vertical side plates are installed around the base of the box-type module of TFB-3 to enhance wave energy dissipation and reduce mooring line tension. In addition, two longitudinal side plates are positioned on the top of the base module. These upper plates serve a dual function: limiting wave overtopping on the top deck and acting as safety barriers. To reduce structural weight, minimize wind resistance, and dissipate any overtopping wave energy, these upper plates are also perforated. The lower perforated side plates are structurally reinforced by three horizontal rib plates within the base of the structure. The hydrodynamic performance of TFB-3 is experimentally

investigated in a wave flume under random wave conditions. The results are compared with the wave-structure interaction characteristics of other FB designs to assess the relative performance of the new model.

2. Methodology

2.1. Prototype Design

The basic dimensions of these breakwaters are calculated and selected based on the empirical formulas proposed by Jones [24], Briggs [25], and Wagner et al. [26]. The prototype of TFB-3 structure can be constructed using reinforced concrete, with its internal voids filled with lightweight materials such as polystyrene, which are commonly used in construction. The primary dimensions of the breakwater box are 20 m in length, 12 m in width, and 5 m in height, respectively (Figure 1). The lower side plates are approximately 1 m in height, while the upper side plates measure 1.5 m. All upper and lower side plates are perforated, with the perforations covering 10% of the total surface area. The wall thickness is set at 25 cm to accommodate two layers of reinforcement. The estimated total weight of a TFB-3 segment is approximately 764 tons. As a result, the draft and freeboard height of a breakwater segment are 4.0 m and 3.5 m, respectively.

2.2. Tested Model

There is no specific standard for determining the appropriate range of model scale values. Hudson et al. [27] proposed an optimal model scale range for FB studies, varying from 1:6 to 1:27. The selection of the model scale depends on the prototype, the experimental wave parameters, and the capacity of the facility. Due to limitations of wave flume capacity, a model scale of 1:20 is selected for this study.

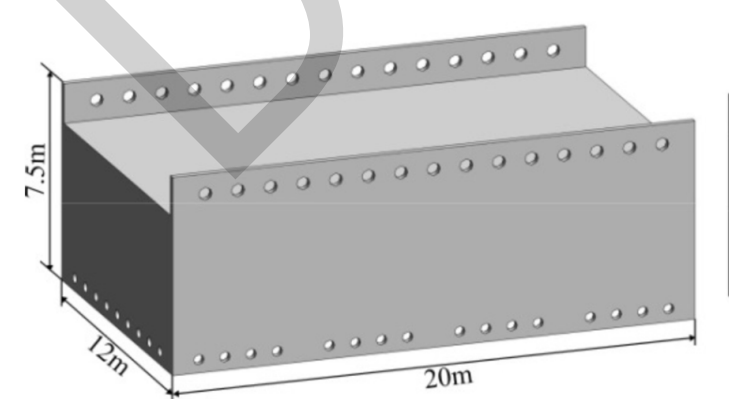
Model TFB-3 is a porous H-type FB consisting of a base box block with dimensions of = 98 cm 60 cm 25 cm. This block is attached to two upper porous vertical plates, each 7.5 cm high, and seven lower porous vertical plates, each 5 cm high (Figure 2). The TFB-3 model has a larger draft due to the inclusion of additional lower porous vertical plates.

This increased draft enhances both the wave attenuation and the stability of the FB model. Details of the test layout for models TFB-1 and TFB-2 are shown in Figure 3 and Figure 4, respectively [21]. To clarify the wave reduction efficiency of the FB models, all models had the same material weight (M), width (B), and length (L), and were tested in similar water depth conditions (D). Moreover, all the test models allowed waves to overtop their crest. The detailed dimensions of all three FB models are provided in Table 1. While the full-scale prototype was constructed from concrete with the surface roughness is, the experimental models were manufactured using 4 mm thick steel sheets coated with paint to replicate the surface roughness of concrete (ranging from 0.0097 to 0.012). This approximation was achieved by applying empirical conversion techniques commonly used in hydraulic model testing. Each model was anchored by four catenary lines, each with a length of 1.4 m and a unit weight of 0.43 kg/m.

2.3. Experimental Setup

The TFB-3 model was tested using a two-dimensional wave flume. The main dimensions of the wave flume were 34 m in length, 1 m in width, and 1 m in height. It consisted of a flat concrete bottom and an 8 mm glass sidewall running along the entire length of the flume. A wave generator without an active wave absorber was set at one end of the flume to generate random waves. Meanwhile, an absorbing beach with an armor layer was placed at the opposite end to prevent wave reflection and transmission. Additionally, an active wave absorber made of a perforated foam panel was installed directly in front of the beach. These structures could absorb more than 95% of the transmitted waves in the flume.

The experimental TFB-3 model was positioned approximately 13 m from the wave maker. The water level at different positions along the wave flume was measured using six wave sensors. A static calibration process with an accuracy of less than 1% was conducted for all six wave gauges at the beginning and end of each experiment set. The first wave gauge, W1, was installed about 5.5 m from



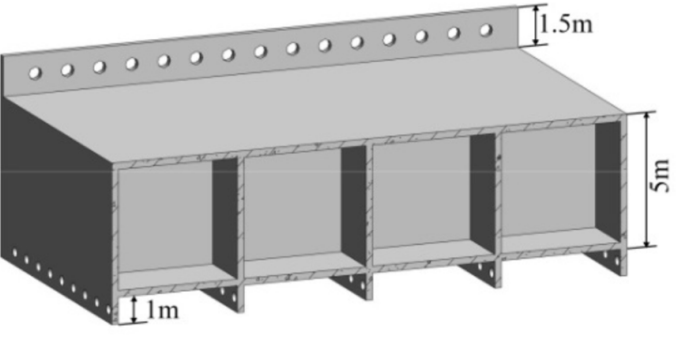


Figure 1. The 3D configuration of the prototype porous H-type floating breakwater (TFB-3)

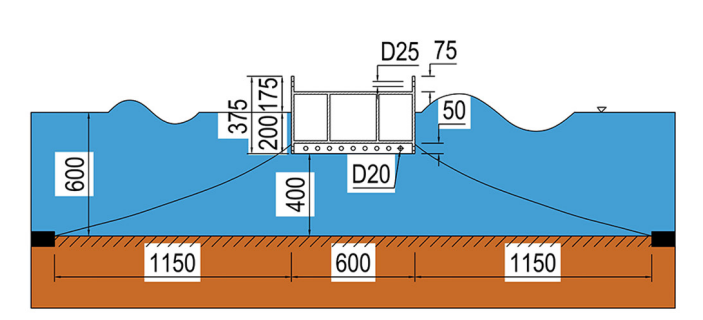




Figure 2. The experimental model of TFB-3 in wave flume (Unit: mm) TFB: Floating breakwater

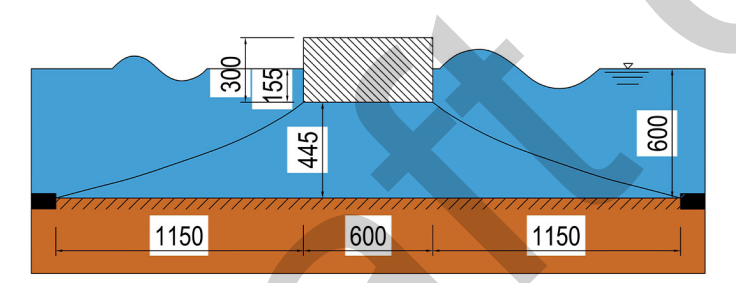
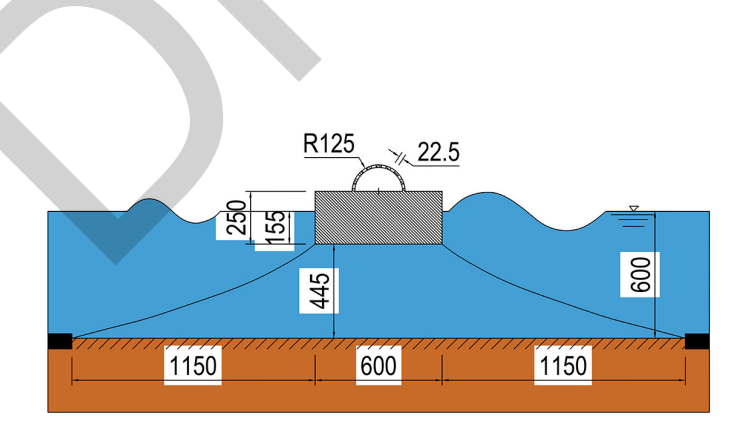
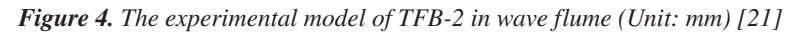


Figure 3. The experimental model of TFB-1 in wave flume (Unit: mm) [21]









Dimensions	TFB-1	TFB-2	TFB-3
Length, L (mm)	980	980	980
Width, B (mm)	600	600	600
Height, H (mm)	300	250	250
Draft, d (mm)	155	155	200
Freeboard, R_c (mm)	145	220	175
Semicircular radius, R (mm)		125	
Height of lower vertical porous plates, s (mm)			50
Height of upper vertical porous plates, $f(mm)$			75
Upper hole diameter, D_u (mm)		22.5	25
Lower hole diameter, D_l (mm)			20
Mass, M (kg)	95.5	95.5	95.5
FB: Floating breakwater			

Table 1. Details of the main dimensions of the tested FB models

the wave maker and approximately four times the longest wavelength produced in the wave flume (about 7.5 m from the FB model) to measure incident wave conditions without disturbances caused by motion response of the structure. Sensors W2, W3, and W4 were installed to measure the reflected waves in front of the FB model using the threepoint method proposed by Mansard and Funke [28]. Wave gauge W4, was positioned approximately 2.5 m seaward from the model, while sensor W3 was set in front of W4 at a distance of 0.4 m, and W2 was set at 0.27 m in front of W3. The spacing between the three wave gauges was adjustable to match each experimental wave peak period, ensuring the most accurate capture of reflected and incident waves. Wave gauge W5 was placed 0.35 m from the centerline of the model to capture the water surface fluctuation at the leading edge of the structure. The last gauge, W6, was positioned 2.5 m behind the model and approximately 10 m from the waveabsorbing beach to measure the waves transmitted through the model. Simultaneous data acquisition and analysis from all wave gauges was conducted using the DHI Wave Synthesizer software installed on a personal computer. This computer, connected to a servo actuator, transferred the wave signal to the generator. Figure 5 presents the configuration of the wave flume.

2.4. Tested Wave Conditions

The tested waves were selected based primarily on the laboratory capacity as well as the typical prototype conditions along the coastal area of Vietnam [29]. Specifically, significant wave heights range from 1.0 to 3.0 m and peak wave periods vary from 6 to 10 seconds in central and southern Vietnam coastal areas. Due to limitations of the wave flume and the wave maker, extreme storm events were not modeled but will be considered in future studies. In this

study, the tested random waves had significant wave heights (H_{\perp}) ranging from 0.05 m to 0.15 m, while the peak wave periods (T_n) varied from 1.1 s to 1.7 s. These correspond to the relative widths $(B/L_{\rm p})$ between 0.25 and 0.5, and wave steepness (Hs/Lp) values from 0.037 to 0.067. A total of 21 tests per model were conducted using random waves generated by a JONSWAP spectrum. Each experiment lasted approximately 1200 seconds (around 1000 waves) with a sampling frequency of 20 Hz. In total, 2400 data points per channel were collected in each test and used for Fast Fourier Transform analysis. The repeatability of results was verified by averaging the results over runs and analyzing the standard deviation, which remained within 5%. Moreover, all experiments were performed with a consistent water depth of 0.6 m, corresponding to a prototype water depth of 12 m. The details of the experiments are summarized in Table 2.

2.5. Analysis Method Of Experimental Results

The reflected and incident waves were separated by applying the three-point method to the measured wave heights at wave gauges W2, W3, and W4. The primary purpose of using this method is to minimize measurement errors in phase and amplitude caused by wave nonlinearity [28]. According to Hales [30], the wave attenuation is denoted by the coefficient of transmission C_r , defined as follows:

$$C_t = \frac{H_t}{H_t} \tag{1}$$

In which H_i is the height of the incident wave, and H_i is the height of the transmitted wave.

Because the wave energy is proportional to the square of the wave height, reducing the wave height by one-quarter leads to a reduction of more than 50% decrease in wave energy [31]. The coefficient of transmission C_t in breakwater designs is primarily determined by the protection requirements of the

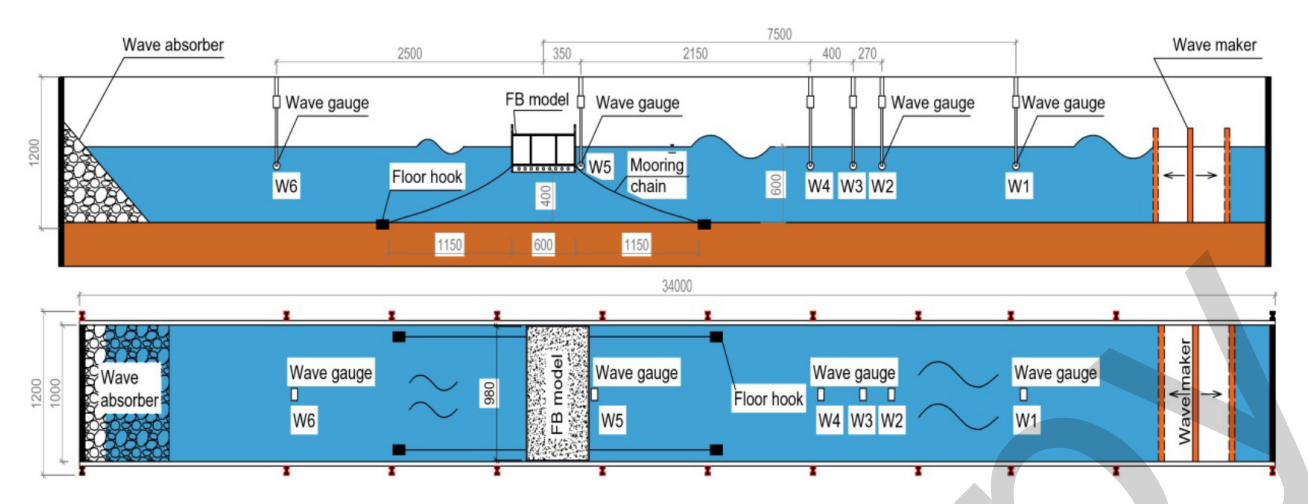


Figure 5. Configuration of the tested models in wave flume and arrangement of wave gauges (Unit: mm) FB: Floating breakwater

Table 2. Details of experimental test conditions

Model	Wave height range (cm)	Wave period range (s)	Number of runs	Time of each run (s)	Water depth (cm)
	4.95-5.15	0.97-1.02	2		
	7.45-7.53	1.28-1.33	2		
TFB-1	9.79-10.22	1.39-1.42	2		
	12.5-12.53	1.6	2		
	14.54-15.31	1.69-1.71	2		
	4.81-5.01	0.92-1.07	2		
	7.48-7.51	1.28-1.35	2		
TFB-2	9.93-10.09	1.35-1.42	3	1200	60
	12.30-12.68	1.60	2		
	14.91-15.09	1.68-1.71	2		
	4.73-5.14	1.07-1.11	3		
	7.49-7.57	1.28-1.35	2		
TFB-3	9.88-10.03	1.35-1.42	2		
	12.40-2.51	1.60	2		
	14.93-15.54	1.70-1.71	2		

target area. For example, coastal sporting and recreational activities require an ideal wave damping level with a C_t value of 0.6. Nevertheless, this value may not be suitable for harbour basin and mooring area calmness requirements. A standard value for the coefficient of wave transmission proposed by Briggs [25] is 0.5 or lower.

Meanwhile, the coefficient of reflection C_r is applied to express the reflection of the waves due to the FB and is determined by the following:

$$C_r = \frac{H_r}{H_i} \tag{2}$$

In which H_i is the incident wave height, and H_r is the reflected wave height. A C_r value of 1 means that the FB reflects the entire incident wave when. In contrast, the value of $C_r = 0$ indicates that the wave reflection does not occur. Meanwhile, wave reflection exists partially if the value of C_r ranges from 0 to 1.

Wave energy dissipated by the FB is also investigated using the coefficient of dissipation proposed by Teh et al. [32].

$$C_d = \sqrt{\frac{E_d}{E_i}} = \sqrt{1 - C_r^2 - C_t^2} = \sqrt{1 - \left(\frac{H_r}{H_i}\right)^2 - \left(\frac{H_t}{H_i}\right)^2}$$
(3)

Where E_i is the energy of incoming wave, and E_d is the dissipated wave energy due to the FB.

Furthermore, the wave climate in front of the breakwaters was also evaluated by utilizing the wave disturbance coefficient (C_p) , as follows:

$$C_f = \frac{H_f}{H_i} \tag{4}$$

Where Hf is the height of the wave in front of the FB. A value of $C_f > 1$ represents an increase of wave height in front of the FB [33]. Conversely, $C_f < 1$ means that the height of the wave in front of the FB is reduced. Meanwhile, $C_f = 1$ indicates that the wave field in front of FB remains unchanged.

Four hydrodynamic coefficients (C_t , C_r , C_d , and C_f) and the relationship of these coefficients with the geometric and incoming wave characteristics were used to evaluate FB performance. Specifically, C_t quantifies transmitted wave height; C_r measures reflected wave energy; C_d assesses energy lost (e.g., turbulence, friction); and C_f indicates surface agitation in front of the structure. These four parameters are widely accepted in the literature as comprehensive for evaluating FB performance [15,22,23,25,32,34,35].

3. Results and Discussion

3.1. Wave Transmission

The previous experimental studies were conducted to assess the influence of geometrical configuration and wave conditions on the transmission of waves of FBs [13,16,20,34-39]. This study evaluates the impact of the incident wave characteristics, including height H_i and peak period T_n , as well as the crest freeboard Rc of FB, on wave transmission of the tested model TFB-3. Figure 6 illustrates the differences in the coefficient of wave transmission (C) among the three models with varying relative crest freeboard (R/H) at the same water depth. The results indicate that the coefficient of wave transmission C_t of the TFB-3 model decreases as the relative crest freeboard increases. Specifically, as the relative crest freeboard of the TFB-3 breakwater increases from 1.13 to 4.73, the C coefficient decreases from 0.5 to 0.3. This trend is consistent with the findings for the TFB-1 and TFB-2 models. The deviation in the TFB-1 curve likely stems from its flat rectangular geometry, which leads to greater sensitivity to overtopping and reflected wave interactions, particularly at higher wave steepness. These findings result in less consistent wave transmission trends compared to the other two models [21]. Moreover, Figure 6 shows that the TFB-3 model is the most effective in wave reduction within the range 2.94<Rc/Hi≤4.77. In the range $1.13 \le \text{Rc/Hi} \le 2.94$, the average C_t values of the TFB-2 and TFB-3 models are higher than those of the TFB-1 model by approximately 16.0% and 5.5%, respectively. Nevertheless,

the TFB-3 model demonstrates superior wave reduction performance when $R_c/H_i > 2.94$. More precisely, the average C_i value of the TFB-3 model is about 17.14% lower than that of the TFB-2 model.

Numerous previous studies have confirmed that the coefficient of wave transmission (C_r) of FBs is significantly influenced by the wave period [14,16,18,20,37,38]. The peak wave period (T_p) is used to determine the wavelength (L_p), which in turn defines the relative breakwater width (B/L_p). As a result, the relative width of the FB (B/L_p) is also considered a critical factor affecting the variation of the C_t value [37]. Figure 7 illustrates the relationship between C_t and B/L_p for the tested TFB-3 model. Additionally, the data on C_t and B/L_p for the TFB-1 and TFB-2 models from [21] are included for comparison. The figure demonstrates that the coefficient of transmission decreases as the relative breakwater width increases for the TFB-3 model. This indicates that increasing the width of the FB enhances its

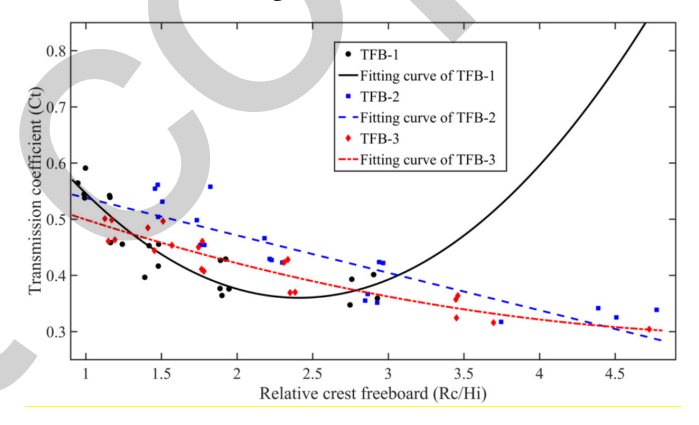


Figure 6. Comparison of wave transmission coefficients (Ct) of TFB-3 with other FB models at different relative crest freeboard (Rc/Hi). black circular dots represent Ct values of TFB-1. blue square dots represent Ct values of TFB-2. Red diamond dots represent Ct values of TFB-3

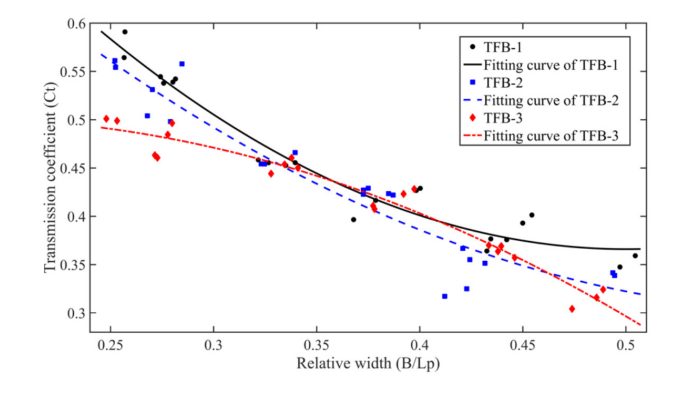


Figure 7. Comparison of wave transmission coefficients (Ct) of TFB-3 with other FB models at different relative widths (B/Lp). Black circular dots represent Ct values of TFB-1; Blue square dots represent Ct values of TFB-2; Red diamond dots represent Ct values of TFB-3

wave attenuation performance, making the TFB-3 model particularly effective in dissipating short-wave energy [21]. Furthermore, Figure 7 highlights that the TFB-3 model exhibits the highest wave attenuation efficiency among the three models, as most of its C_t values are lower than those of the TFB-1 and TFB-2 models under the same conditions. The difference in the magnitude of the coefficient C_t becomes more pronounced in the range of $B/L_p \le 0.3$. Specifically, at $B/L_p = 0.253$, the average coefficients of transmission of the TFB-3 model are approximately 15.6% and 10% lower than those of the TFB-1 and TFB-2 models, respectively. This difference diminishes in the range of $B/L_p > 0.32$, but the average C_t values of the TFB-1 and TFB-2 models remain higher than that of the TFB-3 model.

3.2. Wave Reflection

The efficiency of FBs is also assessed based on wave reflection. High wave reflection can pose risks to ship navigation, particularly when entering harbor basins or mooring areas. For FB projects designed to protect harbor basins and mooring areas, wave reflection is a key criterion in selecting suitable structural options. Figure 8 shows the relationship of the C_{i} and R/H_{i} for the TFB-3 model, with comparisons to the TFB-1 and TFB-2 models. The results indicate that Cr, the coefficient of wave reflection of the TFB-3 model, is significantly influenced by the relative crest freeboard. Specifically, as the relative crest freeboard increases, wave reflection intensifies. This increase in C can be attributed to the higher crest freeboard, which reduces wave overtopping. Consequently, a greater portion of wave energy above the water level is reflected. Among the three models, the TFB-3 model consistently exhibits the lowest coefficient of wave reflection across all relative crest freeboard values. The average values of the coefficient of wave reflection generated by the TFB-3 model are usually lower than those of the TFB-1 and TFB-2 models by approximately 3.9% to 19.1% and 6.5% to 15.2%, respectively. These findings confirm that the TFB-3 model has the best anti-reflective performance among the three models.

The coefficient of wave reflection is influenced not only by the incident wave parameters but also significantly by the geometrical characteristics of the FB structure [13,18,21,40,41]. Figure 9 depicts a comparison of wave reflection coefficient (C_r) for the TFB-3 model at different relative widths (B/L_p) with those of the TFB-1 and TFB-2 models. It can be seen that the increasing trend of C_r is induced by the TFB-3 model across all relative widths (B/L_p) . This suggests that the model effectively predicts C_r variations based on these parameters. This confirms that the wave reflection of the TFB-3 model is strongly dependent on its relative width. However, at the same relative width value of B/L_p , the coefficient of C_r induced by the TFB-3 model

is generally lower than that of the other models. The most significant difference in the coefficient of wave reflection is observed when the relative width B/L_p is less than 0.41, corresponding to a wave period greater than 1.2 s.

3.3. Wave Energy Dissipation

The wave attenuation mechanism during wave-breakwater interactions is intricate and difficult to measure. For this reason, the coefficient of energy dissipation, C_a , is usually used to evaluate the amount of wave energy dissipated by the breakwater. Figure 10 shows the comparison of wave dissipation coefficient C_a , of the TFB-3 model at different values of R_c/H_i with that of the TFB-1 and TFB-2 models. Figure 10 also reveals that the dissipation coefficient of the TFB-1 and TFB-2 models is always lower than that of the TFB-3 model at all relative crest freeboard values. In other words, the TFB-3 model dissipates wave energy most efficiently among the three breakwater models. Specifically,

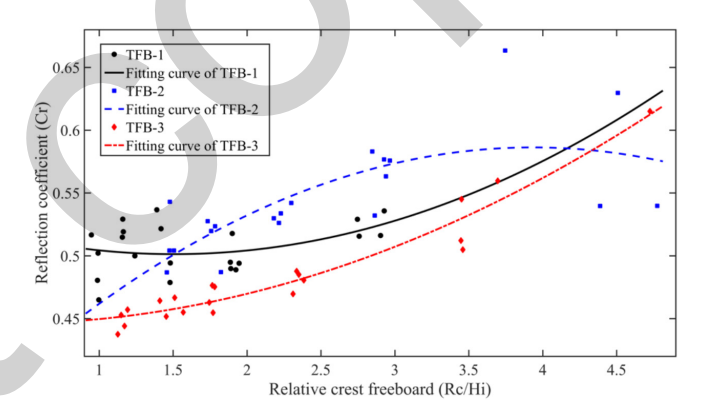


Figure 8. Comparison of wave reflection coefficient (Cr) of TFB-3 with other FB models at different relative crest freeboard (Rc/Hi). Black circular dots represent Cr values of TFB-1; Blue square dots represent Cr values of TFB-2; Red diamond dots, represent the Cr values of TFB-3

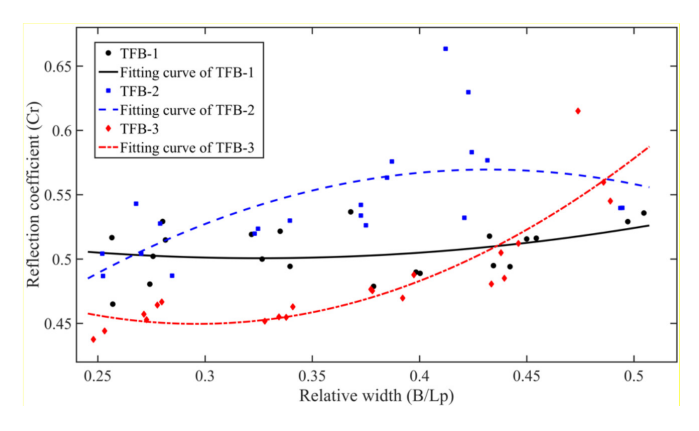


Figure 9. Comparison of wave reflection coefficient (Cr) of TFB-3 with other FB models at different relative width (B/Lp). Black circular dots represent Cr values of TFB-1; Blue square dots represent Cr values of TFB-2; Red diamond dots represent Cr values of TFB-3

the C_d coefficients induced by the TFB-1 and TFB-2 models are approximately 6.1% and 7.2% lower than those of the TFB-3 model. Moreover, Figure 10 shows that the C_d coefficient of the TFB-3 model tends to decrease after the relative crest freeboard exceeds the value of 3.0. This trend is also observed in the TFB-1 model when R_c/H_i exceeds 2.25. Meanwhile, the C_d coefficient of the TBF-2 model inceases as the relative crest freeboard increases.

Figure 11 illustrates the influence of the relative width of B/L_p on the energy dissipation coefficients C_d for the three models. It is again found that the TFB-3 model exhibits superiority in wave energy dissipation across all relative width values, with the most pronounced effect observed when $B/L_p < 0.4$. Additionally, the C_d coefficient of the TFB-3 model increases by only approximately 4% when the relative width is increased by 50%. In contrast, the C_d coefficient of the TFB-1 model and the TFB-2 model increases by approximately 14% and 12.2%, respectively.

3.4. Wave Disturbance in Front of FB

When incident waves encounter a FB, part of the wave energy is reflected towards the open sea, creating a reflected wave (H_i) . Another portion of the wave energy is transmitted through gaps in the breakwater or beneath the FB, producing a transmitted wave (H). Additionally, overtopping may occur, allowing water to pass over the deck of the FB. Furthermore, the motion of the floating structure induces a radiated wave (H_p) , which, in conjunction with the reflected wave, interacts with the incident wave in front of the FB, leading to wave resonance and causing a rise in the water surface at the structure's front. The changes in wave conditions in front of experimental FB models can be assessed using the wave disturbance coefficient C_r . Figure 12 presents a comparison of the coefficient of wave disturbance (C_{ϵ}) of the TFB-3 model at different relative crest freeboards (R/H), alongside those of the TFB-1 and TFB-2 models. The results indicate that the average values of C_f induced by the TFB-1 and TFB-2 models are generally higher than those of the TFB-3 model. Additionally, the trends of the C_f coefficient for the three models exhibit notable differences, as illustrated in Figure 12. Specifically, the C_f coefficient of the TFB-2 model decreases once the relative crest freeboard exceeds 3.0, while it increases in the TFB-3 model beyond this threshold. In contrast, the C_f coefficient of the TFB-1 model gradually rises as the relative crest freeboard increases.

Figure 13 shows the wave disturbance coefficient (C_f) at different relative widths (B/L_p) for the TFB-3 model, compared to the TFB-1 and TFB-2 models. Notably, all C_f coefficients for the TFB-3 model and other models across all experimental scenarios exceed 1.0, indicating an increase in wave activity in front of the structure to varying degrees. In general, the TFB-3 model produces lower C_f values compared

to the other models. Specifically, the C_f coefficients for the TFB-1 and TFB-2 models are consistently higher than those of the TFB-3 model by an average of 1.31%, and 7.03%, respectively, across all values of relative width B/L_p .

3.5. Relationship Between the Hydrodynamic Coefficients and Dimensionless Parameters

As the results presented in the above sections show, the efficiency of FBs is influenced by many parameters, such as incident wave parameters and the dimensions of FBs. The relationship between hydrodynamic coefficients (C_r, C_r, C_d) and the dimensionless parameters $(B/L_p \text{ and } R/H_p)$ can be expressed in the following formula:

$$C_t, C_r, C_d = f\left(\frac{B}{L_p}, \frac{R_c}{H_i}\right) \tag{5}$$

Two simple empirical equations for C_i and C_r as a function of R_c/H_i and B/L_p for each type of FB are derived using regression analysis and recorded data of three types of FBs,

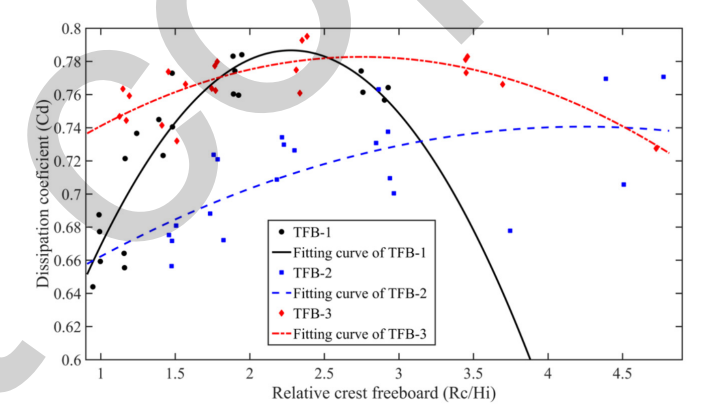


Figure 10. Comparison of wave dissipation coefficient (Cd) of TFB-3 with other FB models at different relative crest freeboard (Rc/Hi). Black circular dots represent Cd values of TFB-1; Blue square dots represent Cd values of TFB-2; Red diamond dots represent Cd values of TFB-3

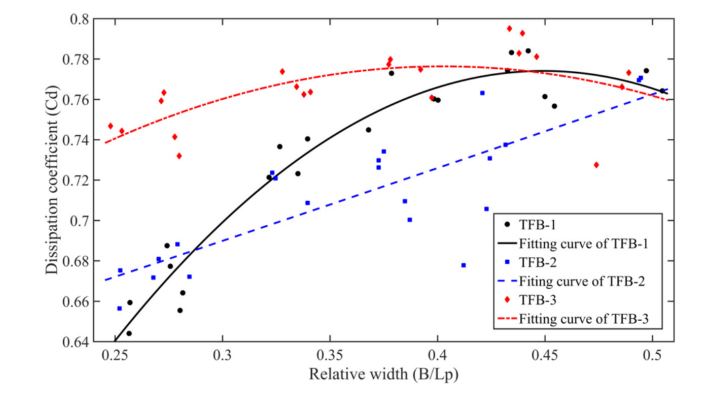


Figure 11. Comparison of wave dissipation coefficient (Cd) of TFB-3 with other FB models at different relative width (B/Lp). Black circular dots represent Cd values of TFB-1; Blue square dots represent Cd values of TFB-2; Red diamond dots represent Cd values of TFB-3

as derived in Equations 6-11. In addition, C_d of three FBs is calculated according to Equation (3).

$$C_t^{TFB-1} = -1.509 \left(\frac{B}{L_p}\right) + 0.08 \left(\frac{R_c}{H_i}\right) + 0.868$$
 (6)

$$C_r^{TFB-1} = -0.043 \left(\frac{B}{L_p}\right) + 0.015 \left(\frac{R_c}{H_i}\right) + 0.497$$
 (7)

$$C_t^{TFB-2} = -0.908 \left(\frac{B}{L_D}\right) - 0.007 \left(\frac{R_c}{H_i}\right) + 0.78$$
 (8)

$$C_r^{TFB-2} = -0.059 \left(\frac{B}{L_p}\right) + 0.031 \left(\frac{R_c}{H_i}\right) + 0.486$$
 (9)

$$C_t^{TFB-3} = 0.549 \left(\frac{B}{L_p}\right) - 0.017 \left(\frac{R_c}{H_i}\right) + 0.657$$
 (10)

$$C_r^{TFB-3} = -0.108 \left(\frac{B}{L_p}\right) + 0.048 \left(\frac{R_c}{H_i}\right) + 0.418$$
 (11)

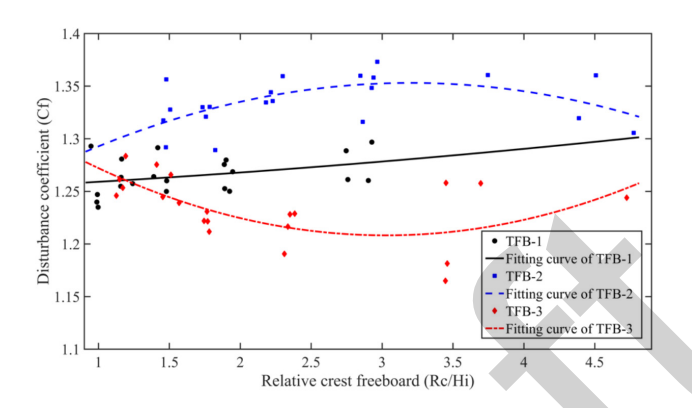


Figure 12. Comparison of wave disturbance coefficient (Cf) of TFB-3 with other FB models at different relative crest freeboard (Rc/Hi). black circular dots represent Cf values of TFB-1; blue square dots represent Cf values of TFB-2; red diamond dots represent Cf values of TFB-3

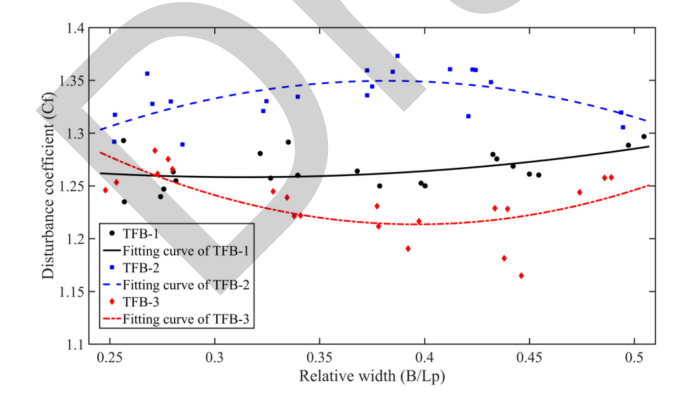


Figure 13. The comparison of the wave disturbance coefficient (Cf) of TFB-3 with other FB models is conducted at different relative widths (B/Lp). Black circular dots represent Cf values of TFB-1; Blue square dots represent Cf values of TFB-2; Red diamond dots represent Cf values of TFB-3

The estimated values from Eqsuations 6-11 were compared with the experimented results using the correlation coefficient R-squared (R²), Mean Absolute Error (MAE) and Mean Squared Error (MSE). Table 3 summarizes the R², MAE and MSE values for three models (TFB-1, TFB-2, and TFB-3). A good agreement was observed for the C_r coefficient across all three models, with the values of R² ranging between 0.89 and 0.96 (Table 2). Although the R² values of the coefficient of wave reflection C_r are lower than those of the coefficient of wave transmission C_r , the empirical formulas for the coefficient of wave reflection C_r remain acceptable and reliable, as indicated by the relatively low MAE and MSE values. The validity of Equations 6-11 applies within the ranges of $0.248 \le B/L_p \le 0.497$ and $0.947 \le R/H_r \le 4.774$.

4. Conclusion

This research presents the experimental results on wave-structure interaction for a newly modified porous H-type FB (TFB-3). A series of two-dimensional wave flume experiments were conducted to evaluate the wave dissipation effectiveness of the TFB-3 model under random wave conditions. The performance of the TFB-3 model was compared with that of the conventional TFB-1 and the modified TFB-2 designs in all four hydrodynamic indicators. Key insights include:

- 1. The smallest values of C_t induced by the TFB-3 model range from 0.3 to 0.5, which is lower than those of the TFB-1 and TFB-2 models by approximately 7.4% and 4.0%, respectively.
- 2. The lowest values of C_r are observed in the TFB-3 model, with the TFB-1 and TFB-2 models being higher by approximately 11.5% and 10.9%, respectively.
- 3. With the values of C_d ranging from 0.73 to 0.80, the TFB-3 model causes the highest energy dissipation among all models.
- 4. Among the three models, the TFB-3 model induces the lowest wave disturbance in front of the structure. The average

Table 3. The performance indices of the empirical equations for the TFB-3 model and other FB models

No.	Type	Coefficient	\mathbb{R}^2	MAE	MSE
1	TFB-1	C_{t}	0.96	0.014	2.510-4
2		C_{r}	0.32	0.016	3.310-4
3	TFB-2	C_{t}	0.89	0.021	7.010-4
4		C_{r}	0.63	0.023	1.010-3
5	5 6 TFB-3	C _t	0.95	0.012	2.010-4
6		C _r	0.90	0.011	1.810-4

MAE: Mean Absolute Error, MSE: Mean Squared Error, FB: Floating breakwater, R^2 : R-squared

values of the C_f coefficient for the TFB-1 and TFB-2 models exceed those of the TFB-3 model by approximately 1.31% and 7.03%, respectively.

- 5. Empirical formulas were employed to estimate the coefficients of wave transmission and reflection. These empirical results demonstrate good agreement with the experimental data.
- 6. The innovative use of perforated vertical plates in the TFB-3 model to reduce overtopping and turbulence.

These findings support the feasibility of TFB-3 for real-world coastal applications, particularly in soft-soil regions. Future work should evaluate storm condition response and mooring forces under dynamic loads.

Footnotes

Authorship Contributions

Concept design: M. T. Vu, and Q. H. Vu, Data Collection or Processing: M. T. Vu, and Q. H. Vu, Analysis or Interpretation: M. T. Vu, and Q. H. Vu, Literature Review: A.-D. Nguyen, and T. Mai, Writing, Reviewing and Editing: M. T. Vu, A.-D. Nguyen, and T. Mai.

Funding: The financial support from Vietnam Ministry of Transport (DT214006).

References

- S. K. Ramnarayan, S. A. Sannasiraj, and V. Sundar, "Hydrodynamic performance of pile supported breakwaters - a review," *APAC 2019*, pp. 929-935, Sep 2019.
- [2] W. H.Tutuarima and K. d'Angremond, "Cost comparison of breakwater types," *Coastal Engineering Proceedings*, vol. 1, pp. 1934-1944, 1998.
- [3] IPCC, The physical science basis, in sixth assessment report (AR6). 2021. https://www.ipcc.ch/report/ar6/wg1
- [4] T. D. Nguyen, T. N. Phan, and S. Likitlersuang, "Evaluating the applicability of large-diameter cement deep mixing method for soft ground improvement: a landmark case study in Vietnam," *International Journal of Geosynthetics and Ground Engineering*, vol. 11, article number 19, 2025.
- [5] P. Pongvithayapanu, and S. Teachavorasinskun, "Local site response on simulated strong earthquake motion at laem chabang port, Thailand," *Journal of Southeast Asian Applied Geology*, vol. 2, pp. 242-250, Dec 2010.
- [6] L. P. Dong, T. Aoyama, Y. Yamada, K. Iwama, and M. Nakanishi, "A low improvement ratio cement deep mixing in combination with cement pipe mixing method for large scale reclamation at Patimban Port development project," *Japanese Geotechnical Society Special Publication*, vol. 11, pp. 272-277, Nov 2024.
- [7] M. M. Zakaria, K. M. Hafez, W. H. El Kamash, and A. H. Moubarak, "stabilization of soft clay soil by deep mixing," *Life Science Journal*, vol. 17, pp. 1-15, Mar 2020.
- [8] A. Kamath, A. Sasikumar, and H. Bihs, "Numerical study of wave interaction with a submerged porous breakwater in combination with a floating breakwater," *Coastal Engineering Proceedings*, vol. 1, Dec 2018.

- [9] V. M. Tuan, N. V. Thanh, and N. T. Viet, "Predicting the effect of submerged breakwaters on hydrodynamics and sediment transportcase study of Ba Lang Beach (Nha Trang, Vietnam)," in APAC 2019, Hanoi, Vietnam: Springer Singapore, 2019.
- [10] L. H. Trung, N. V. Tuan, T. T. Tung, D. T. Linh, N. T. Duy, and B. Duong, "Experimental assessment of wave reduction possibility of porous concrete blocks," *Journal of Science and Technology in Civil Engineering (STCE) HUCE (In Vietnamese)*, vol. 15, pp. 44-54, 2021.
- [11] R. Ranasinghe, and I. L. Turner, "Shoreline response to submerged structures: a review," *Coastal Engineering*, vol. 53, pp. 65-79, Jan 2006
- [12] H. H. Sao, and N. V. Dung, "The physical model of floating breakwater deal with the efficient decrease of wave level to protect marinas and small harbours," *Journal of Water Resources and Environmental Engineering (In Vietnamese)*, 2011.
- [13] H. M. Teh, V. Venugopal, and T. Bruce, "Hydrodynamic performance of a free surface semicircular perforated breakwater," Proceedings of 32nd Conference on Coastal Engineering, Shanghai, China, 2011.
- [14] H. M. Teh, M. Azizan, V. J. Kurian, and A. Hashim, "Use of a floating breakwater system as an environmentally friendly method of coastal shelter," *WIT Press*, vol. 148, pp. 309-318, Sep 2015.
- [15] I. H. Cho, "Transmission coefficients of a floating rectangular breakwater with porous side plates," *International Journal of Naval Architecture and Ocean Engineering*, vol. 8, pp. 53-65, Jan 2016.
- [16] C. Y. Ji, X. Chen, J. Cui, O. Gaidai, and A. Incecik, "Experimental study on configuration optimization of floating breakwaters," *Ocean Engineering*, vol. 117, pp. 302-310, 2016.
- [17] N. T. Trung, "Assessment of wave reduction effect of anchored pier type floating structure for berth," *Journal of Science and Technology in Civil Engineering (STCE) HUCE (In Vietnamese)*, vol. 12, 2018.
- [18] M. R. Gesraha, "Analysis of Π shaped floating breakwater in oblique waves: I. Impervious rigid wave boards," *Applied Ocean Research*, vol. 28, pp. 327-338, Oct 2006.
- [19] E. D. Christensen, H. B. Bingham, A. P. Skou Friis, A. K. Larsen, and K. L. Jensen, "An experimental and numerical study of floating breakwaters," *Coastal Engineering*, vol. 137, pp. 43-58, Jul 2018.
- [20] Y. N. Zheng, X. M. Liu, C. P. Chen, Y. P. Jiang, and C. W. Zhang, "Experimental study on the wave dissipation performance and mooring force of porous floating breakwater," IOP Conference Series: Earth and Environmental Science, vol. 189, 022058, 2018.
- [21] V. M. Tuan, B. Duong, V. Q. Hung, N. D. Manh, and N. M. Linh, "Experimental study on the wave dissipation performance of a perforated semi-circular floating breakwater," *Journal of Science and Technology in Civil Engineering (STCE) HUCE*, vol. 16, pp. 59-70, Jun 2022.
- [22] Y. S. Shen, J. N. Pan, Z. Y. R. Zhou, and X. G. Wang, "Experimental study on wave attenuation performance of a new type of floating breakwater with twin pontoons and multi porous vertical plates," *China Ocean Engineering*, vol. 36, pp. 384-394, Jul 2022.
- [23] K. Z. Hu, T. J. Xu, and S. Wang, "Hydrodynamic investigation of a new type of floating breakwaters integrated with porous baffles," *Applied Ocean Research*, vol. 154, 104380, Jan 2025.

- [24] D. B. Jones, "Transportable breakwater a survey of concepts," Naval Civil Engineering Laboratory, 1971.
- [25] M. J. Briggs, "Performance characteristics of a rapidly installed breakwater system," in Technical Report No 01-13, U.S. Army Engineer Research and Development Center: Vickburg, MS, Jul 2001. https://apps.dtic.mil/sti/citations/ADA395021
- [26] H. Wagner, A. Gotz, R. Reinsch, and H. J. Kaiser, "Schwimmende wellenbrecher im einsatz in einem tagenbaurestsee mitteldeutschlands," *Binnenschifffahrt ZfB*, 2011. [In German]
- [27] R. Y. Hudson, F. A. Herrmann, and R. A. Sager, "Coastal hydraulics models," U.S. Army Waterways Experiment Station, 3909 Halls Ferry Road, Vicksburg, MS United States 39180-6199, 1979.
- [28] E. P. D. Mansard, and E. R. Funke, "The measurement of incident and reflected spectra using a least squares method," *Coastal Engineering*, pp. 154-172, 1980.
- [29] V. M. Tuan, N. V. Thanh, B. Duong, and V. Q. Hung, "Estimation of wave characteristics in the coastal waters of Vietnam using ERA-Interim model data," *Transport and Communications Science Journal*, vol. 73, pp. 552-573, Jun 2022.
- [30] L. Z. Hales, "Floating breakwaters: state-of-the-art literature review," Technical report no 81-1, DTIC Document, Oct 1981.
- [31] B. O. Tobiasson, and R. C. Kollmeyer, "Marinas and small craft harbors," New York: Springer Science and Business Media, 1991.
- [32] H. M. Teh, V. Venugopal, and T. Bruce, "Hydrodynamic characteristics of a free-surface semicircular breakwater exposed to irregular waves," *Journal of Waterway, Port, Coastal, and Ocean Engineering*, vol. 138, pp. 149-163, 2012.
- [33] H. M. Teh, "Hydrodynamic performance of free surface semicircular breakwaters," Ph.D. dissertation, The University of Edinburgh, 2012.

- [34] Y. C. Guo, S. C. Mohapatra, and C. G. Soares, "Experimental performance of multi-layered membrane breakwaters," *Ocean Engineering*, vol. 281, 114716, Aug 2023.
- [35] F. He, J. Pan, J. Li, S. Zheng, and Z. Yuan, "An experimental study of a rectangular floating breakwater with flexible curtains as wave-dissipating components," *Applied Ocean Research*, vol. 152, 104185, Nov 2024.
- [36] E. Koutandos, P. Prinos, and X. Gironella, "Floating breakwaters under regular and irregular wave forcing: reflection and transmission characteristics," *Journal of Hydraulic Research*, vol. 43, pp. 174-188, Jan 2005.
- [37] E. Peña, J. Ferreras, and F. Sanchez-Tembleque, "Experimental study on wave transmission coefficient, mooring lines and module connector forces with different designs of floating breakwaters," *Ocean Engineering*, vol. 38, pp. 1150-1160, Jul 2011.
- [38] C. Y. Ji, X. Chen, J. Cui, Z. M. Yuan, and A. Incecik, "Experimental study of a new type of floating breakwater," *Ocean Engineering*, vol. 105, pp. 295-303, Jul 2015.
- [39] J. Cui, H. Liu, X. Deng, S. Tao, and Q. Li, "An experimental study on hydrodynamic performance of a box-floating breakwater in different terrains," *Journal of Marine Science and Technology*, vol. 25, pp. 991-1009, Dec 2020.
- [40] S. F. Abdullah, A. Fitriadhy, M. H. Mohd, and A. Jusoh "Hydrodynamic performance of cylindrical floating breakwater in waves," *International Journal of Automotive and Mechanical Engineering*, vol. 14, pp. 4715-4729, Dec 2017.
- [41] J. M. Zhan, X. B. Chen, Y. J. Gong, and W. Q. Hu, "Numerical investigation of the interaction between an inverse t-type fixed/floating breakwater and regular/irregular waves," *Ocean Engineering*, vol. 137, pp. 110-119, Jun 2017.